

 Open access • Journal Article • DOI:10.1103/PHYSREVLETT.90.057401

## Optical properties of gold nanorings — Source link

Javier Aizpurua, Per Hanarp, Duncan S. Sutherland, Mikael Käll ...+2 more authors

**Institutions:** National Institute of Standards and Technology, Chalmers University of Technology, Donostia International Physics Center

**Published on:** 03 Feb 2003 - Physical Review Letters (American Physical Society)

**Topics:** Localized surface plasmon, Plasmon and Colloidal gold

Related papers:

- [A hybridization model for the plasmon response of complex nanostructures.](#)
- [Optical Constants of the Noble Metals](#)
- [Sensing Characteristics of NIR Localized Surface Plasmon Resonances in Gold Nanorings for Application as Ultrasensitive Biosensors](#)
- [Probing Single Molecules and Single Nanoparticles by Surface-Enhanced Raman Scattering](#)
- [The Optical Properties of Metal Nanoparticles: The Influence of Size, Shape, and Dielectric Environment](#)

Share this paper:    

View more about this paper here: <https://typeset.io/papers/optical-properties-of-gold-nanorings-w2igraqteu>

## Optical Properties of Gold Nanorings

J. Aizpurua,<sup>1</sup> P. Hanarp,<sup>2</sup> D. S. Sutherland,<sup>2</sup> M. Käll,<sup>2</sup> Garnett W. Bryant,<sup>1</sup> and F. J. García de Abajo<sup>3</sup>

<sup>1</sup>National Institute of Standards and Technology, Gaithersburg, Maryland 20899-8423

<sup>2</sup>Department of Applied Physics, Chalmers University of Technology, S-41296 Göteborg, Sweden

<sup>3</sup>Centro Mixto CSIC-UPV/EHU and Donostia International Physics Center (DIPC), Apartado 1072, 20080 San Sebastián, Spain  
(Received 13 August 2002; published 3 February 2003)

The optical response of ring-shaped gold nanoparticles prepared by colloidal lithography is investigated. Compared to solid gold particles of similar size, nanorings exhibit a redshifted localized surface plasmon that can be tuned over an extended wavelength range by varying the ratio of the ring thickness to its radius. The measured wavelength variation is well reproduced by numerical calculations and interpreted as originating from coupling of dipolar modes at the inner and outer surfaces of the nanorings. The electric field associated with these plasmons exhibits uniform enhancement and polarization in the ring cavity, suggesting applications in near-infrared surface-enhanced spectroscopy and sensing.

DOI: 10.1103/PhysRevLett.90.057401

PACS numbers: 78.67.Bf, 61.46.+w, 73.20.Mf

Metal nanoparticles exhibit a wide variety of optical phenomena [1] that have made them the center of considerable recent attention. Nanoparticles can be used to guide, enhance, emit, and modify optical fields, phenomena that can be used for novel technological applications such as photonic crystals [2], sensors based on surface-enhanced Raman scattering (SERS) [3–5] and near-field microscopy [6]. The optical response of a particular nanoparticle depends on its size and shape, which defines the intrinsic modes [7], as well as on the local dielectric environment [8]. Interparticle coupling typically leads to energy shifts and splitting of degenerate modes, an effect that is prominent for regular arrays of nanoparticles [9] and can be utilized for the production of efficient SERS substrates [10], or as an electromagnetic probe for atomic scale objects in a scanning tunneling microscopy cavity [11].

In this Letter, we report on tunable optical modes and associated electromagnetic field confinement effects in Au nanorings with radii of the order  $\approx 60$  nm. We emphasize the intrinsic surface plasmon resonances (SPR) of the rings, which are experimentally observed by recording the extinction spectra of disordered layers of identical nanoparticles deposited on glass substrates. We demonstrate that the SPR wavelength can be tuned by varying the thickness of the ring walls, which determines the electromagnetic coupling between the inner and outer ring surfaces. It is argued that this phenomenon is analogous to electromagnetic coupling effects in thin metal films and nanoshells [12,13]. As a support for this interpretation, we present detailed electrodynamic calculations that essentially reproduce the experimentally measured extinction spectra. The calculations also show that a sizable and remarkably uniform field enhancement effect occurs in the ring interior.

The Au rings are produced on soda-glass substrates using colloidal lithography according to the following procedure.

(i) Polystyrene (PS) colloidal particles (110 nm sulphate modified latex) are deposited by electrostatic self-assembly onto the glass substrates. (ii) A 15 to 40 nm thick gold film is evaporated onto the particle coated glass substrates. The thickness of this film controls the thickness  $d$  of the ring walls while the size of the PS particles determines the inner radius. (iii) Ar ion beam etching is then used to remove the Au film, during which secondary sputtering of material creates a gold shell around the sides of the PS particles. (iv) The remainder of the PS particles are removed by a UV-ozone treatment and subsequent water rinse, resulting in free standing Au nanorings.

For comparison, we also produced Au nanodisks by reversing the order of steps (i) and (ii), and by changing the shape of the PS particles by heat pretreatment to avoid the secondary buildup of material around the PS particle. The morphology of the samples were determined by scanning electron microscopy (SEM) and atomic force microscopy. All rings and disks had the same outer radius  $\approx 60$  nm while the heights were  $\approx 40$  and  $\approx 20$  nm, respectively. The thickness of the ring walls was determined independently through side-view SEM images [see Fig. 1(a)]. Normalized optical extinction spectra were measured in a spectrophotometer using unpolarized light incident normal to the nanoparticle substrate.

The bulk nature of the disks is clearly seen in the SEM top view of Fig. 1(b), whereas the corresponding nanoring image in Fig. 1(c) shows an empty space surrounded by uniform walls. The close-up SEM image in Fig. 1(a) shows that the rings are slightly bulging outwards, a shape derived from the sphericity of the PS particles. Figures 1(b) and 1(c) also shows that the disk and ring samples exhibit approximately the same particle density,  $1.4$  and  $1.7 \times 10^9$  particles/cm<sup>2</sup>, respectively. As the sampling area of the extinction measurement was approximately  $0.7$  cm<sup>2</sup>, the optical data are averaged over  $\approx 10^9$  particles.

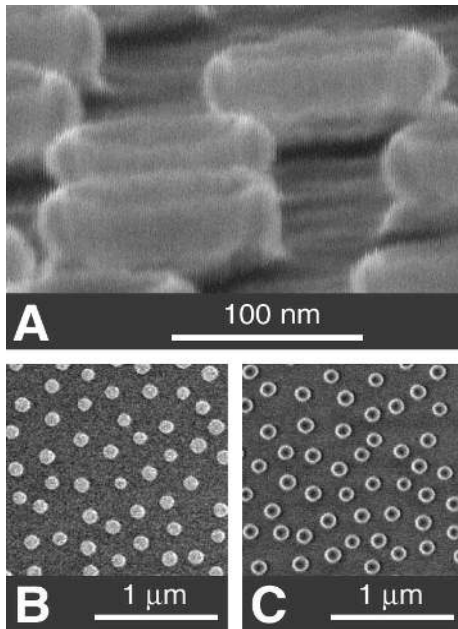


FIG. 1. SEM images of gold nanorings and nanodisks prepared by colloidal lithography. (a)  $80^\circ$  tilt image of a ring structure. The walls of the rings are thin enough for the 30 keV electrons to pass through. (b),(c) Top views of disks and rings taken at an acceleration voltage of 1.5 keV. The heights of the disks and rings in the figure are  $\approx 20$  and  $\approx 40$  nm, respectively, whereas the radius is  $\approx 60$  nm in both cases. The thickness of the ring walls was estimated to  $14 \pm 2$  nm from side-view SEM images similar to (a).

Figure 2(a) shows experimental extinction spectra for disks and rings derived from the measured transmittance  $T = I/I_o$ , where  $I_o$  is the intensity of the incident light and  $I$  is the intensity of the transmitted light. The experimental cross section  $\sigma_{\text{ext}}$  is estimated from  $I - I_o = -\sigma_{\text{ext}}NI_o$ , where  $N$  is the 2-dimensional particle density. While the disks show an SPR peak well below 1000 nm (dashed curve), the nanorings exhibit near-infrared extinction peaks with a center wavelength extremely sensitive to the ratio between the ring thickness and radius  $d/a$ . For a constant external ring radius of  $a = 60$  nm, a redshift of almost 400 nm is observed by reducing the ratio  $d/a$  from 0.22 to 0.16 [i.e., from  $r_1$  to  $r_3$  in Fig. 2(a)]. This shift is larger than the shifts induced by the interparticle interaction in close-packed nanoparticle arrays [9].

In order to elucidate the character of the SPR modes, numerical calculations of the extinction cross section for both types of particles (disks and rings) were performed for the geometrical parameters mentioned above. The dielectric functions for Au and substrate, i.e.  $\text{SiO}_2$ , were taken from Ref. [14]. Maxwell's equations were solved using the boundary element method [15], in which the electromagnetic field is expressed in terms of charges and currents distributed on the surfaces and interfaces of the structure under consideration. The customary boundary conditions for the electromagnetic field provide a set of

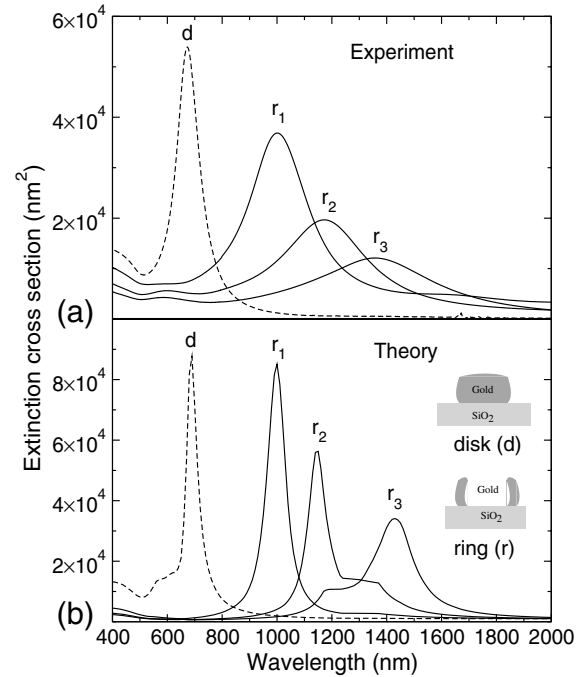


FIG. 2. (a) Experimental extinction spectra of disks (d, dashed line) and rings (r, solid lines). The estimated wall thickness  $d$  of the rings is  $d = 14 \pm 2$  nm ( $r_1$ ),  $d = 10 \pm 2$  nm ( $r_2$ ), and  $d = 9 \pm 2$  nm ( $r_3$ ), respectively. (b) Calculated extinction spectra for the same particles as in (a). The rings exhibit near-infrared features at larger wavelengths for thinner walls. The disks show a dipolar excitation at around 700 nm.

linear integral equations, with charges and currents as unknowns, which are solved self-consistently in the presence of the external incident-light field by discretizing the integrals. In Fig. 2(b), the calculated extinction cross sections are plotted vs  $\lambda$  for disks (d) and for rings of different thickness as in the experiments ( $r_1$  to  $r_3$ ). The agreement between experiment and theory is excellent, both in terms of the peak positions and in the absolute and relative weights of the different surface plasmon resonances. The peak widths increase with decreasing wall thickness in both the experiments and in the theoretical model, although the calculated widths are clearly smaller than the measured ones in all cases. For the case of the rings, the calculations clearly indicate that even a small spread in  $d$  would give rise to a relatively large distribution of peak positions. It is thus likely that the large experimental peak widths are a result of inhomogeneous broadening, due to a finite distribution of wall thickness for the measured samples.

The large difference in the SPR position for disks and rings can be understood by analyzing the particular modes that are most efficiently excited for each type of particle. The extinction spectrum of disklike particles is dominated by a dipolar ( $l = 1$ ) mode, whose frequency depends on the particle size due to retardation effects in the intraparticle electromagnetic interaction [16]. As the

particle size increases, the different multipolar modes shift to the red according to a dispersion similar to the one shown in Fig. 3(a), where we have used a Drude-like dielectric function appropriate for Au (see caption). This particular calculation was performed for the lowest order modes of a spherical particle of radius  $a$ , for which analytical formulas are available through the simplified Mie theory [16]. Although the exact mode positions differ between a disklike object and a sphere, the redshift with increasing size is maintained. However, for the small diameters under consideration here ( $a\omega_p/c < 1$ ), the redshift is not substantial.

Turning to the nanorings, there is a strong electromagnetic coupling between the inner and outer ring walls when the thickness  $d$  is small compared to the ring radius  $a$ . This leads to a new scheme of polarization and results in mode splitting [see Fig. 3(b)] similar to the case of a thin metallic slab, which is characterized by symmetric and antisymmetric mode branches. In the long-wavelength limit, appropriate to the particle sizes and wavelengths under discussion, the dispersion relation of

the modes of a slab described by the Drude-like dielectric function given in the caption of Fig. 3 reduces to

$$(\omega_{\pm})^2 = \omega_p^2 \frac{1 \pm e^{-kd}}{(\epsilon_o + \epsilon_s) \pm e^{-kd}(\epsilon_o - \epsilon_s)}, \quad (1)$$

where  $\omega_{\pm}$  corresponds to the symmetric ( $-$ ) and anti-symmetric ( $+$ ) mode frequencies,  $k$  is the wave vector, and  $d$  is the slab thickness. The effect of the  $\text{SiO}_2$  substrate has been qualitatively incorporated by surrounding the slab with a medium of dielectric function  $\epsilon_s = 2.12$ . In the present case, the wave vector  $k$  is related to the ring circumference  $2\pi a$  by  $k = \frac{2\pi n}{2\pi a} = n/a$ , where  $n$  is the order of the mode. This relationship is illustrated in Fig. 3(b) for the first three ( $n = 1 - 3$ ) symmetric ( $\omega_-$ ) and antisymmetric ( $\omega_+$ ) modes of a *slablike* ring. As the thickness of the walls increases, the modes converge to the surface plasmon mode of a planar surface  $\omega_s = \omega_p/\sqrt{\epsilon_o + \epsilon_s}$ . If the wall thickness is decreased instead, the symmetric modes redshift and eventually go to zero in the  $d \ll a$  limit. This pattern of oscillation corresponds to a charge distribution with the same sign at the inner and outer surfaces of the wall, as shown in Fig. 3(b). It is the symmetric  $n = 1$  mode that is responsible for the near-infrared excitations observed in the nanorings, and accounts for the  $d/a$  dependence evident in the experimental and theoretical results shown in Fig. 2. The polarization pattern of this mode can be understood as a strong dipolar excitation that involves the entire ring perimeter, and where equal sign charges at opposite sides of the wall interact to a degree determined by the wall thickness. On the contrary, the antisymmetric branches correspond to patterns of oscillation of opposite sign along both walls.

An estimate of the peak position for the gold nanorings made from Eq. (1) by defining  $a \approx 60$  nm and  $d/a \approx 0.1$  results in a near-infrared wavelength  $\lambda \approx 1110$  nm. This is in general agreement with both the experiments and the more detailed calculations presented in Fig. 2. The simple analytical model [Eq. (1)] thus qualitatively explains the observed extinction spectra. However, the effect of the vertical truncation of the ring, the fact that the wall surfaces are not parallel, and the actual configuration of the ring-substrate system lead to additional corrections that are correctly described by the numerical calculation presented in Fig. 2(b). In addition, the interaction between the upper and lower ring edges lowers the mode frequencies in comparison to an infinitely long ring. This effect has been confirmed by our calculations, although it is not included in the simple analytical model. The dependence on ring height is not as dramatic as the dependence on the  $d/a$  ratio.

Nanorings could serve as resonant nanocavities for holding and probing smaller nanostructures, such as biomolecules or quantum dots. We show in Fig. 4(a) the near-field vector distribution and field enhancement ( $|E|/|E_{\text{inc}}|$ ) in a horizontal plane through the middle of the  $r_1$  nanoring modeled in Fig. 2. The incident

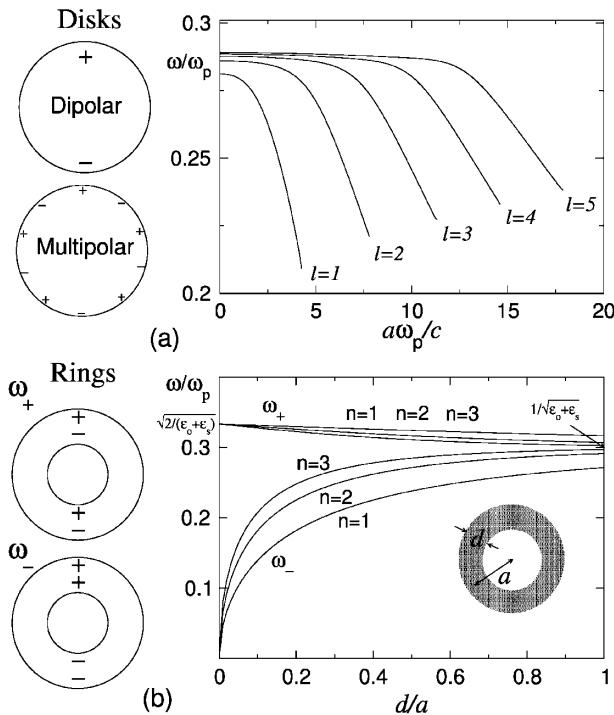


FIG. 3. (a) Left: top view of dipolar and multipolar charge density patterns for disks. Right: dispersion of the lowest-order modes in a spherical particle of radius  $a$  characterized by a Drude-like dielectric function,  $\epsilon = \epsilon_o - \omega_p^2/\omega^2$ . The values  $\omega_p = 8$  eV and  $\epsilon_o = 9 + 5i$  were chosen to qualitatively represent gold in the spectral region under investigation. (b) Left: top view of the charge-density pattern in a nanoring for the antisymmetric ( $\omega_+$ ) and symmetric ( $\omega_-$ ) modes. Right: mode frequencies of nanorings as a function of  $d/a$  in the long-wavelength limit. The rings are characterized by the same Drude-like dielectric function as in (a) and surrounded by a material with dielectric function  $\epsilon_s = 2.12$ .

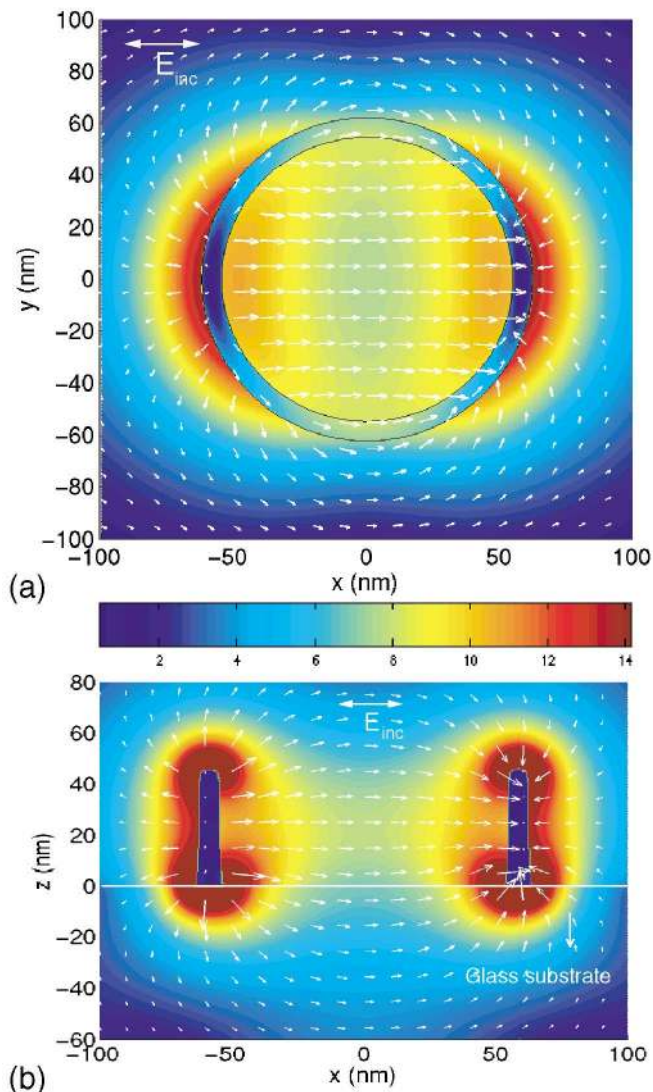


FIG. 4 (color). (a) Horizontal cut of the near field distribution and field enhancement ( $|E|/|E_{inc}|$ ) for a ring of radius  $a = 60$  nm and wall thickness  $d = 10$  nm at  $z = 22.7$  nm. The scale bar shows the field enhancement. (b) Vertical cross section of the same ring for  $y = 0$  nm. The maximum value of  $|E|/|E_{inc}|$  is 50. All values above 14 are indicated in brown for (b). The wavelength chosen corresponds to the peak of the extinction spectrum  $\lambda = 1000$  nm. The polarization vector is indicated by arrows and the incident light is propagating downwards in (b).

wavelength is in resonance with the first symmetric mode ( $\lambda = 1000$  nm). The electric field is substantially enhanced inside the ring cavity (green and yellow regions, corresponding to  $|E|/|E_{inc}| \approx 8-10$ ), where it is rather homogeneous. The field distribution in a plane that contains the ring axis [Fig. 4(b)] shows that the uniform enhancement is maintained through most of the cavity region even though the ring height is less than  $1/2$  the ring diameter. The enhancement factor reaches a maximum of  $|E|/|E_{inc}| \approx 50$  at the upper and lower ends of the ring,

indicating a buildup of charge at these ends which supports the field enhancement uniformly in the cavity. Combined with the tunability of the peak position through the  $d/a$  ratio, the enhancement effects indicate potential applications in nonlinear optical phenomena (e.g., switching and all-optical transistors) as well as in improved near-infrared SERS sensitivity.

In summary, it has been shown that ringlike nanoparticles exhibit tunable plasmon resonances in the near infrared that are not observed for solid particles of similar size. The volume confined by the nanoring is empty and therefore accessible to various sensing and spectroscopy applications at the nanometer scale. The experimentally observed optical response of these structures is well described by numerical simulations and the main features can be qualitatively understood from simple models of the charge oscillation patterns. The predictive character of these calculations allows one to tailor the shape of a particle in order to achieve excitation spectra on demand with controlled field enhancement.

- [1] U. Kreibig and M. Volmer, *Optical Properties of Metal Clusters*, Springer Series in Material Science Vol. 25 (Springer-Verlag, Berlin, 1995).
- [2] K. Sakoda, *Optical Properties of Photonic Crystals*, Springer Series in Optical Sciences Vol. 80 (Springer-Verlag, Berlin, 2001).
- [3] S. Nie and S.R. Emory, *Science* **275**, 1102 (1997).
- [4] K. Kneipp *et al.*, *Phys. Rev. Lett.* **78**, 1667 (1997).
- [5] H. Xu, E.J. Bjerneld, M. Käll, and L. Börjesson, *Phys. Rev. Lett.* **83**, 4357 (1999).
- [6] D.W. Pohl and D. Courjon, *Near Field Optics*, NATO ASI, Ser. E (Kluwer, Dordrecht, 1993), Vol. 241.
- [7] C.F. Bohren and D.R. Huffman, *Absorption and Scattering of Light by Small Particles* (John Wiley & Sons Inc., New York, 1998).
- [8] T.R. Jensen, J.C. Schatz, and R.P. Van Duyne, *J. Phys. Chem. B* **103**, 2394 (1999).
- [9] B. Lamprecht, G. Schider, R.T. Lechner, H. Ditlbacher, J.R. Krenn, A. Leitner, and F.R. Aussenegg, *Phys. Rev. Lett.* **84**, 4721 (2000).
- [10] A. Wei, B. Kim, B. Sadtler, and S.L. Tripp, *Chem. Phys. Chem.* **2**, 743 (2001).
- [11] J. Aizpurua, G. Hoffmann, S.P. Apell, and R. Berndt, *Phys. Rev. Lett.* **89**, 156803 (2002).
- [12] S.J. Oldenburg, J.B. Jackson, S.L. Wescott, and N.J. Halas, *Appl. Phys. Lett.* **75**, 2897 (1999).
- [13] J.B. Jackson and N.J. Halas, *J. Phys. Chem. B* **105**, 2743 (2001).
- [14] E.D. Palik, *Handbook of Optical Constants of Solids* (Academic Press, New York, 1985).
- [15] F.J. García de Abajo and A. Howie, *Phys. Rev. Lett.* **80**, 5180 (1998); *Phys. Rev. B* **65**, 115418 (2002).
- [16] R. Ruppin, in *Electromagnetic Surface Modes*, edited by A.D. Boardman (John Wiley & Sons Ltd., New York, 1982), p. 349.